TECHNICAL NOTE
« IMPROVEMENT OF BRIGHTNESS TEMPERATURE MODELS FOR EARTH-SPACE PATHS»

	Name, CNES entity	Date and Signature
Prepared by	**Xavier BOULANGER** **DSO/RF/ITP** **Specialist in RF Propagation in charge of tropospheric propagation thematic**	Boulanger Xavier Signature numérique de Boulanger Xavier Date : 2021.05.06 11:57:07 +02'00'
Verified by	**Bouchra BENAMMAR** **DSO/RF/ITP** **Specialist in RF and Optical Propagation**	Benammar Bouchra Signature numérique de Benammar Bouchra DN : c=FR, o=CNES, ou=0002 775665912, ou=Agents CNES, 2.5.4.45=benammb@cnes.fr, cn=Benammar Bouchra Date : 2021.05.06 14:22:24 +02'00'
Authorised by	**Clément DUDAL** **Head of DSO/RF/ITP Division**	Dudal Clement Signature numérique de Dudal Clement DN : c=FR, o=CNES, ou=0002 775665912, ou=Agents CNES, 2.5.4.45=dudalc@cnes.fr, cn=Dudal Clement Date : 2021.05.06 14:03:53 +02'00'

INTERNAL/EXTERNAL DISTRIBUTION LIST			
CNES entity/ Company Organisation	**Name (+email address if external)**	**Observation for**	
		Action	**Information**
DSO/RF/D	D. PRADINES		x
DSO/RF/DA	C. LAPORTE		x
DSO/RF/ITP	ALL		x
DSO/NT/ST	ALL		x
ONERA	L. CASTANET (Laurent.Castanet@onera.fr)		x

INDEXATION

Authors: **Xavier BOULANGER**		
Title/Scope: This technical note describes CNES internal research activities on downwelling brightness temperature models for Earth-Space paths between 1 and 200 GHz.		
Configuration management: **No**	Date:	By :
Contract : **Not applicable**		

MODIFICATION DIRECTORY

Issue	Date	Evolutions
1.0	**09/03/2021**	Creation

TERMS, DEFINITIONS AND ABBREVIATIONS

Acronym : Abbreviation	Definition
CCDF	Complementary Cumulative Distribution Function
DEM	Digital Elevation Model
ECMWF	European Centre for Medium-Range Weather Forecasts
GEO	Geostationary Earth Orbit
ITU-R	International Telecommunication Union – Radiocommunication Sector
ILWC	Integrated Liquid Water Content (total columnar content of cloud liquid water)
ISL	Inter-Satellite Link
IWVC	Integrated Water Vapour Content (total columnar content of water vapour)
Ka-band	20-30 GHz (space communications)
Ku-band	10-14 GHz (space communications)
LEO	Low Earth Orbit
Q/V-band	40-50 GHz (space communications)
SG3	Study Group 3 of ITU-R
W-band	70-90 GHz (space communications)

VARIABLES MEMO

Variable	Definition	Unit
φ	Latitude	°N
λ	Longitude	°E
θ	Elevation	°
f	Frequency	GHz
p	Probability of exceedance (for a CCDF)	%
Z	Geometric height (above mean sea level)	km
H	Geopotential height (above mean sea level)	km
h_s	Height above mean sea level of the surface of the Earth	km
P	Total pressure	hPa
P_s	Total pressure at the surface of the Earth	hPa
$\overline{P_s}$	Mean of P_s for a given period (e.g. annual or monthly mean)	hPa
T	Temperature	K
T_s	Temperature at the surface of the Earth	K
$\overline{T_s}$	Mean of T_s for a given period (e.g. annual or monthly mean)	K
ρ_w	Water vapour density	g/m^3
ρ_{w_s}	Water vapour density at the surface of the Earth	g/m^3
$\overline{\rho_{w_s}}$	Mean of ρ_{w_s} for a given period (e.g. annual or monthly mean)	g/m^3
ρ_l	Cloud liquid water density	g/m^3
γ_o	Oxygen specific attenuation	dB/km
A_O	Attenuation due to oxygen	dB
γ_w	Water vapour specific attenuation	dB/km
A_W	Attenuation due to water vapour	dB
γ_c	Cloud liquid water specific attenuation	dB/km
A_C	Attenuation due to clouds	dB
A_{tot}	Total attenuation ($A_{tot} = A_O + A_W + A_C$)	dB
$T_{B,down}$	Net downwelling microwave brightness temperature	K
T_{mr}	Mean radiating temperature	K
T_c	Exoatmospheric cosmic microwave background blackbody temperature	K

TABLE OF CONTENTS

1 INTRODUCTION

1.1 OBJECT AND CONTENT OF THE DOCUMENT

This technical note describes CNES internal research activities on downwelling brightness temperature models for Earth-Space paths between 1 and 200 GHz. It presents a revision to the existing recommended prediction method in Section 3.2 of Part 3 of Recommendation ITU-R P.372-14 (the method is also recalled in Section 3 of Recommendation ITU-R P.618-13). The existing prediction method predicts the location- and frequency-**independent** average downwelling radio (sky) noise temperature and mean radiating temperature of the Earth's atmosphere under non-rainy conditions (i.e. due to atmospheric gases and clouds). The revised prediction method predicts the location- and frequency-**dependent** average and statistical distributions of the downwelling brightness temperature of the Earth's atmosphere.

The content of this technical note is the following:

- Section 2 reminds the main information given in [RD 6] in which new reference atmospheric profiles have been derived from the up-to-date ECMWF reanalysis database, ERA5.
- Section 3 gives a brief analysis on the impact of area on the surface of the Earth for regular latitude/longitude grids. This is a key point for the development and the global test of propagation models.
- Section 4 provides a framework for new prediction methods of the instantaneous net downwelling microwave brightness temperature and the statistical distribution of the net downwelling microwave brightness temperature. In particular, the maps of the mean annual vertical atmospheric profiles are used to develop a new model of the **mean radiating temperature** from 1 to 200 GHz. The performances of the new models are assessed with a comparison to radiosounding observations.

1.2 CONTEXT

This study falls within the tropospheric propagation thematic roadmaps of the division DSO/RF/ITP.

ITU-R SG3, and in particular Working Parties 3J, 3M, and 3L have recently approved several roadmaps on the improvement of the prediction methods of Earth-Space propagation. Among all ITU-R SG3 Recommendations, one is of interest:

- ITU-R P.372-14 which provides prediction methods for radio noise

1.3 DOCUMENTATION

1.3.1 APPLICABLE DOCUMENTS

Reference	Title
AD 1 : FdR_Propa_RF_Tropo	Tropospheric propagation thematic roadmap, internal CNES document
AD 2 : Programme d'Intérêt Commun	Déclaration de lancement de la phase 2 du Programme d'Intérêt Commun (PIC) PERF: Propagation Electromagnétique Radio-Fréquence, 24/01/2020

1.3.2 REFERENCE DOCUMENTS

Reference	Title
RD 1 : ITU-R P.372-14	Recommendation ITU-R P.372-14, “Radio noise” , Geneva, August 2019
RD 2 : ITU-R P.676-12	Recommendation ITU-R P.676-12, “Attenuation by atmospheric gases and related effects”, Geneva, August 2019
RD 3 : ITU-R P.835-6	Recommendation ITU-R P.835-6, “Reference standard atmospheres”, Geneva, December 2017
RD 4 : ITU-R P.836-6	Recommendation ITU-R P.836-6, “Water vapour: surface density and total columnar content”, Geneva, December 2017
RD 5 : ITU-R P.840-8	Recommendation ITU-R P.840-8, “Attenuation due to clouds and fog” , Geneva, August 2019
RD 6 : DSO/RF/ITP-2020.0032915	X. Boulanger, “Improvement of the Tropospheric Propagation Instantaneous and Statistical Models for Earth-Space Paths, Issue 2.0, January 2021

2 NEW REFERENCE DATABASE OF ATMOSPHERIC PROFILES

In [RD 6], a methodology to derive the atmospheric profiles parameters from the new ERA5 ECMWF reanalysis database has been described. New digital maps of the mean (annual, seasonal, monthly) vertical atmospheric profiles have been provided and they were used to develop new prediction methods of gaseous and cloud attenuation.

According to the WMO definition of the climate normals, the new worldwide digital maps of the mean (annual, seasonal, monthly) vertical atmospheric profiles have been derived from 30 years (from 1991 to 2020) of monthly averaged profiles. The maps consist of weighted means (by the number of days in the considered month) of a given parameter (temperature, water vapour density, cloud liquid water density and altitude) for a given pressure level.

As examples, Figure 2-1, Figure 2-2, and Figure 2-3 show the mean annual vertical profiles of temperature, water vapour density, and cloud liquid water density derived from the ERA5 monthly averaged database (1991-2020).

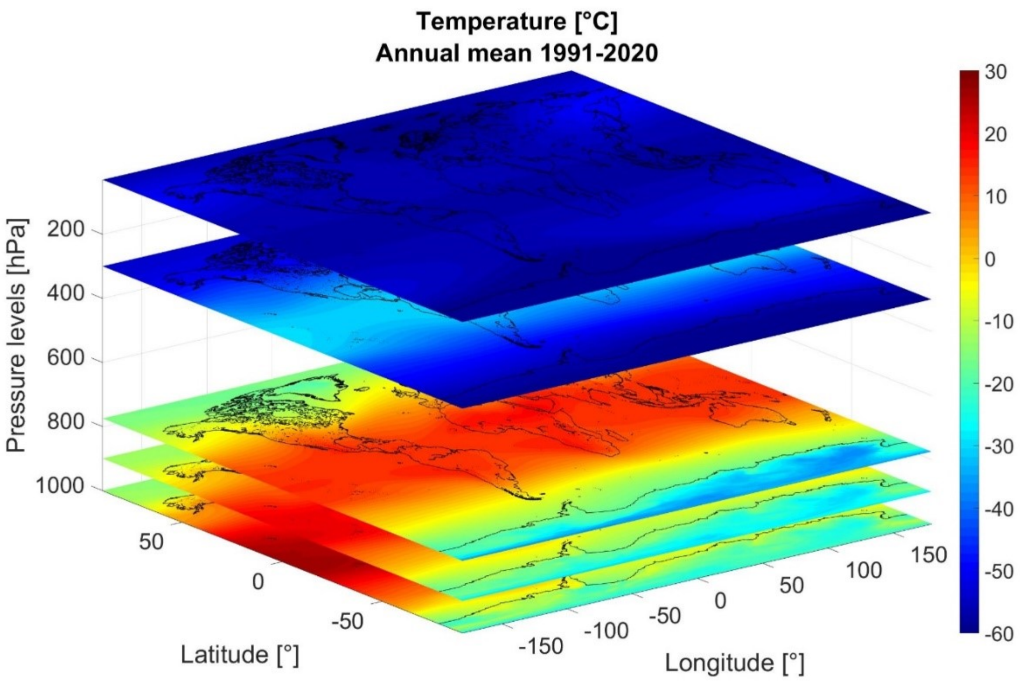

Figure 2-1 : Mean annual vertical profiles of temperature derived from the ERA5 monthly averaged database (1991-2020)

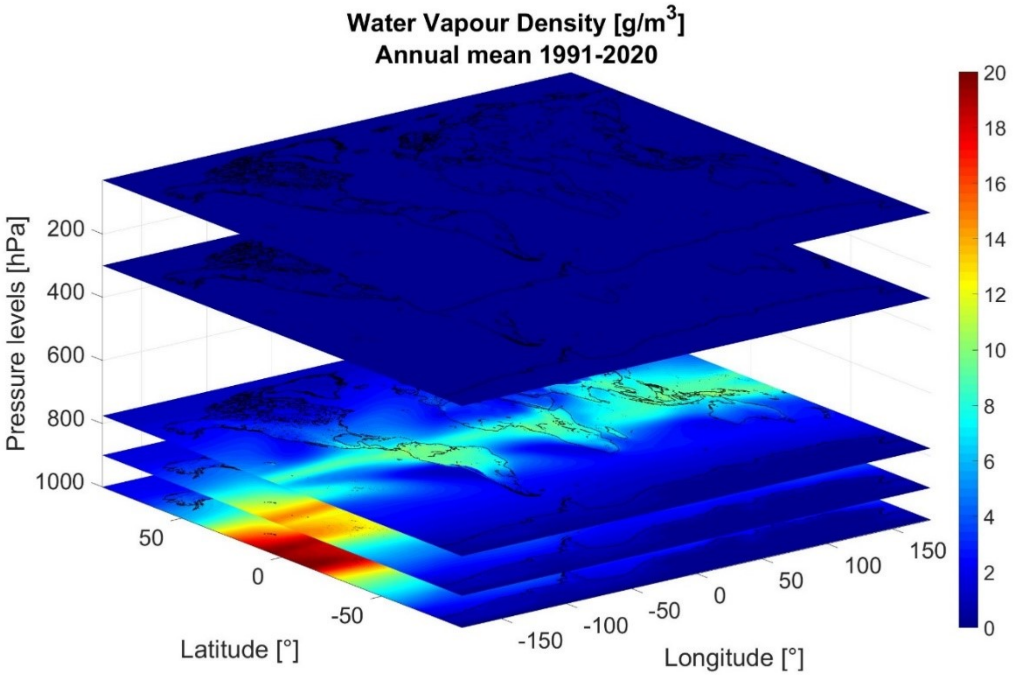

Figure 2-2 : Mean annual vertical profiles of water vapour density derived from the ERA5 monthly averaged database (1991-2020)

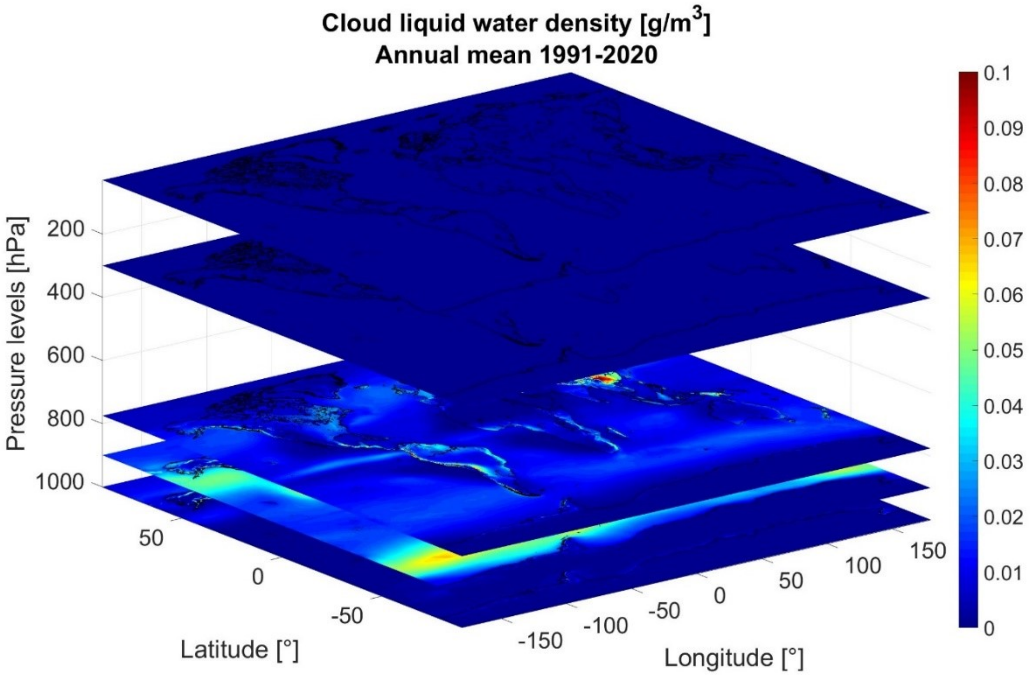

Figure 2-3 : Mean annual vertical profiles of cloud liquid water density derived from the ERA5 monthly averaged database (1991-2020)

3 IMPACT OF AREA ON THE SURFACE OF THE EARTH FOR REGULAR LATITUDE/LONGITUDE GRIDS

One of the main drawbacks of using regular grids in latitude and longitude for both the development and the test of global propagation prediction methods is the fact that the weight of each grid point is the same. However, the area on the surface of the Earth for a given grid cell is increasing from the equator to the poles. It means that the weight given to the grid point on the equator should be more important than over the poles. The area *A* (km) of a latitude(φ)-longitude(λ) rectangle is:

$$A = \frac{\pi}{180} \cdot R_E^2 \cdot \; |\sin\varphi_1 - \sin\varphi_2| \cdot |\lambda_1 - \lambda_2|$$

where R_E is the Earth radius.

For the WGS84 ellipsoid, the distance from the Earth's centre to a point on the spheroid surface at geodetic latitude φ is given by:

$$R_E = R_E(\varphi) = \sqrt{\frac{(a^2\cos\varphi)^2 + (b^2\sin\varphi)^2}{(a\cos\varphi)^2 + (b\sin\varphi)^2}}$$

where a = 6378.137 km and b = 6356.7523142 km.

It can be verified that $R_E(0) = a$ and $R_E(90) = b$.

Noting $\Delta\varphi = \varphi_1 - \varphi_2$ and $\Delta\lambda = \lambda_1 - \lambda_2$ the grid cell resolution in latitude and longitude respectively, the area *A* (km) for a given latitude φ can then be computed from:

$$A(\varphi) = \frac{\pi}{180} \cdot R_E^2(\varphi) \cdot \left|2\sin\frac{\Delta\varphi}{2}\cos\varphi\right| \cdot |\Delta\lambda|$$

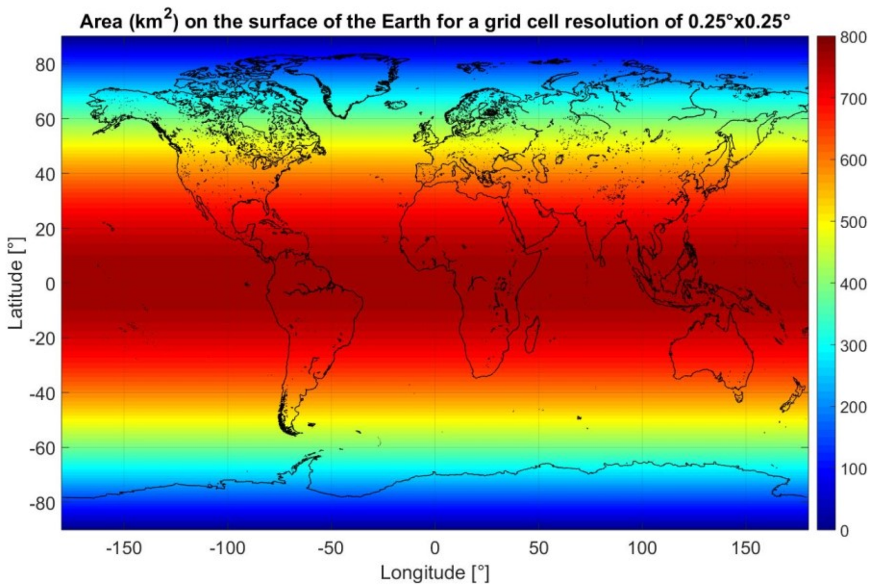

Figure 3-1 : Area (km^2) on the surface of the Earth for a grid cell resolution of 0.25°x0.25°

4 NEW PREDICTION METHOD OF BRIGHTNESS TEMPERATURE

MAIN OBJECTIVES OF SECTION 4.1:

- Description of the theoretical background for the computation of the net downwelling microwave brightness temperature and the mean radiating temperature

MAIN OBJECTIVES OF SECTION 4.2:

- Use of the ERA 5 maps of the mean annual vertical atmospheric profiles to develop a new model of the **mean radiating temperature** for the prediction of the net downwelling microwave brightness temperature from the attenuation on the slant path
- Verification and comparison of the performances of the new model with the prediction method described in Section 3.2 of Part 3 of Recommendations ITU-R P.372-14
- Test of the new model using radiosounding observations

MAIN OBJECTIVES OF SECTION 4.3:

- Derivation of a new prediction method of the statistical distribution of the net downwelling microwave brightness temperature from the statistical distribution of total attenuation on the slant path

4.1 THEORETICAL BACKGROUND

Most of the information given in this section about the computation of the downwelling space-to-Earth microwave brightness temperature looking up are detailed in Section 4 of Annex 1 of ITU-R P.676-12 [RD 2]. It mainly assumes that the atmosphere is composed of successive layers for which layer 1 is typically at the surface of the Earth, and layer k is at the top of the atmosphere.

4.1.1 PLANCK ADJUSTMENT

For a given frequency f (in GHz), the microwave brightness temperature of the jth layer, T_{B_j} (in K), is defined by:

$$T_{B_j} = T_B(f, T_j) = 0.048 \cdot f \cdot \frac{1}{e^{\frac{0.048\, f}{T_j}} - 1}$$

where T_j is the physical temperature of the jth layer. Using the Planck constant, *h* (in J.s), and the Boltzmann constant, *k* (in J/K), we have $\frac{h}{k} = \frac{6.62607015\times10^{-34}}{1.380649\times10^{-23}} = 0.048 \times 10^{-9}$ which is in accordance with the above equation.

T_{B_j} can be well-approximated by T_j for $f < 0.42\,T_j$. For a given frequency f, as the physical temperature, T, increases, the difference between T and the microwave brightness temperature of a blackbody source, T_B, tends towards $0.024f$ (i.e. $T - T_B \rightarrow 0.024f$).

4.1.2 DOWNWELLING MICROWAVE BRIGHTNESS TEMPERATURE

The noise model of an attenuating element with numerical loss L_{elt} ($0 \leq L_{elt} \leq 1$) and physical temperature T_{elt} is as follows:

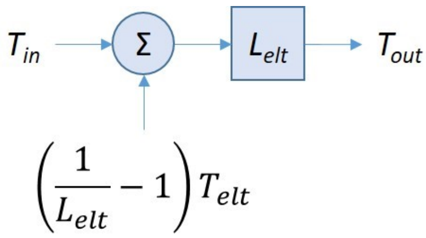

Then, $T_{out} = \left[T_{in} + \left(\frac{1}{L_{elt}} - 1\right) T_{elt}\right] L_{elt} = T_{in} L_{elt} + (1 - L_{elt}) T_{elt}$.

Now assuming k atmospheric layers and ignoring the Planck adjustment for the microwave brightness temperature in a first step, the downwelling sequence is as follows:

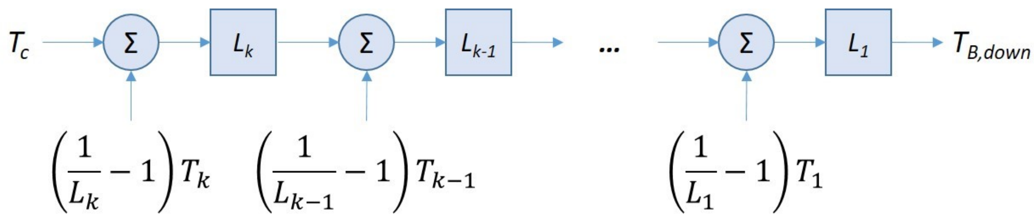

where T_c=2.73 K is exoatmospheric cosmic microwave background blackbody temperature, T_j is still the temperature of the j^{th} layer, and L_j is the numerical loss ($0 \leq L_j \leq 1$) of the j^{th} layer. Hence, the net downwelling microwave brightness temperature, $T_{B,down}$ (in K), is:

$$T_{B,down} = T_c \prod_{j=k}^{1} L_j + \sum_{j=k}^{1} \left[\left(\frac{1}{L_j} - 1\right) T_j \prod_{i=j}^{1} L_i \right] = T_c \prod_{j=1}^{k} L_j + \sum_{j=1}^{k} \left[\left(\frac{1}{L_j} - 1\right) T_j \prod_{i=1}^{j} L_i \right]$$

Noting that $L_j = 10^{-\frac{\gamma_j a_j}{10}}$, where γ_j is the specific attenuation of the j^{th} layer (in dB/km), a_j is the path length through the j^{th} layer (in km), then:

$$\frac{1}{L_j} = 10^{\frac{\gamma_j a_j}{10}}$$

$$\prod_{j=1}^{k} L_j = 10^{-\frac{\sum_{j=1}^{k} \gamma_j a_j}{10}}$$

Finally, if the profiles of pressure, temperature, water vapour and cloud liquid water density along the path are known, and now taking into account the Planck adjustment for the microwave brightness temperature, the net downwelling microwave brightness temperature, $T_{B,down}$ (in K), in absorbing conditions is:

$$T_{B,down}(f) = T_B(f,T_c)10^{-\frac{\sum_{j=1}^{k}\gamma_j a_j}{10}} + \sum_{j=1}^{k}\left[\left(10^{\frac{\gamma_j a_j}{10}} - 1\right)T_B(f,T_j)10^{-\frac{\sum_{i=1}^{j}\gamma_i a_i}{10}}\right]$$

An illustration of the results of the net downwelling microwave brightness temperature between 1 and 1000 GHz is given in Figure 4-1. The computation has been performed using the 6 reference standard atmospheres of Annex 1 of Recommendation ITU-R P.835-6 [RD 3].

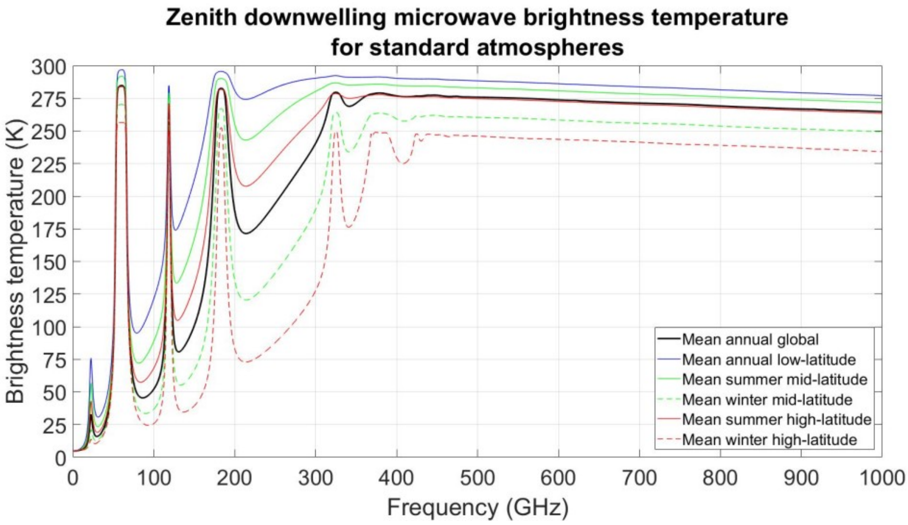

Figure 4-1 : Zenith downwelling brightness temperature (1-1000 GHz)

As this document will focus between 1 and 200 GHz only, Figure 4-2 highlights the results between 1 and 200 GHz.

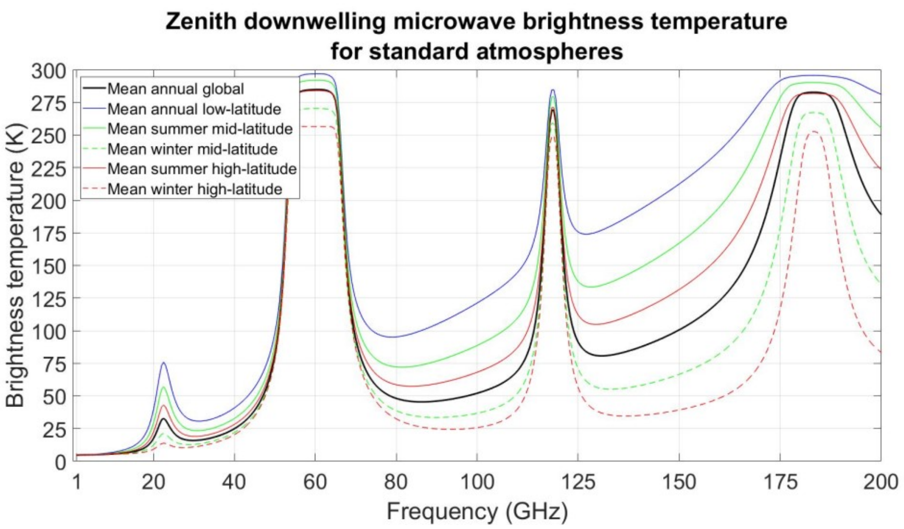

Figure 4-2 : Zenith downwelling brightness temperature (1-200 GHz)

NB: Figure 4-1 and Figure 4-2 only consider atmospheric gases (because no reference cloud profiles are given in Recommendation ITU-R P.835-6) but they are only given as examples. In the following, clouds will be considered.

4.1.3 MEAN RADIATING TEMPERATURE

In Section 4.1.2, it has been shown that the net downwelling microwave brightness temperature can be retrieved by:

$$T_{B,down}(f) = T_B(f,T_c)10^{-\frac{\sum_{j=1}^{k}\gamma_j a_j}{10}} + \sum_{j=1}^{k}\left[\left(10^{\frac{\gamma_j a_j}{10}} - 1\right)T_B(f,T_j)10^{-\frac{\sum_{i=1}^{j}\gamma_i a_i}{10}}\right]$$

which is equivalent to:

$$T_{B,down}(f) = T_B(f,T_c)10^{-\frac{\sum_{j=1}^{k}\gamma_j a_j}{10}} + \frac{\sum_{j=1}^{k}\left[\left(10^{\frac{\gamma_j a_j}{10}} - 1\right)T_B(f,T_j)10^{-\frac{\sum_{i=1}^{j}\gamma_i a_i}{10}}\right]}{\sum_{j=1}^{k}\left[\left(10^{\frac{\gamma_j a_j}{10}} - 1\right)10^{-\frac{\sum_{i=1}^{j}\gamma_i a_i}{10}}\right]}\sum_{j=1}^{k}\left[\left(10^{\frac{\gamma_j a_j}{10}} - 1\right)10^{-\frac{\sum_{i=1}^{j}\gamma_i a_i}{10}}\right]$$

It can be noticed that:

$$\sum_{j=1}^{k}\left[\left(10^{\frac{\gamma_j a_j}{10}} - 1\right)10^{-\frac{\sum_{i=1}^{j}\gamma_i a_i}{10}}\right] = \sum_{j=1}^{k}\left[\frac{1-L_j}{L_j}\prod_{i=1}^{j}L_i\right] = 1 - L_1 + (1-L_2)L_1 + (1-L_3)L_1L_2 + \cdots + (1-L_k)L_1L_2L_3\ldots L_{k-1}$$

$$= 1 - L_1L_2L_3\ldots L_{k-1}L_k = 1 - \prod_{j=1}^{k}L_j = 1 - 10^{-\frac{\sum_{j=1}^{k}\gamma_j a_j}{10}}$$

Consequently, the net downwelling microwave brightness temperature can also be retrieved by:

$$T_{B,down}(f) = T_B(f,T_c)10^{-\frac{A_{tot}(f)}{10}} + T_{mr}(f)\left(1 - 10^{-\frac{A_{tot}(f)}{10}}\right)$$

where $A_{tot}(f)$ is the total attenuation along the path in absorbing conditions (by analogy to Section 4.1.2, $A_{tot}(f) = \sum_{j=1}^{k}\gamma_j a_j$) and T_{mr} is the mean radiating temperature defined by:

$$T_{mr}(f) = \frac{\sum_{j=1}^{k}\left[\left(10^{\frac{\gamma_j a_j}{10}} - 1\right)T_B(f,T_j)10^{-\frac{\sum_{i=1}^{j}\gamma_i a_i}{10}}\right]}{\sum_{j=1}^{k}\left[\left(10^{\frac{\gamma_j a_j}{10}} - 1\right)10^{-\frac{\sum_{i=1}^{j}\gamma_i a_i}{10}}\right]}$$

Finally, knowing the net downwelling microwave brightness temperature, the mean radiating temperature, and the total attenuation along the path (in absorbing conditions) can be reciprocally retrieved by:

$$A_{tot}(f) = 10 \cdot log10\left(\frac{T_{mr}(f) - T_B(f, T_c)}{T_{mr}(f) - T_{B,down}(f)}\right)$$

Section 3.2 of Part 3 of ITU-R P.372-14 [RD 1] proposes a method to predict the mean radiating temperature, T_{mr}. When the surface temperature T_s (K) is known, it may be estimated for clear and cloudy weather as:

$$T_{mr}(f) = T_{mr} = 37.34 + 0.81 \cdot T_s$$

So, the prediction method of Section 3.2 of Part 3 of ITU-R P.372-14 is frequency independent. Moreover, this prediction method also approximates $T_B(f, T_c) \sim T_c$ (i.e. ignoring Planck adjustment) resulting into :

$$T_{B,down_{simplified}}(f) = T_c 10^{-\frac{A_{tot}(f)}{10}} + T_{mr}\left(1 - 10^{-\frac{A_{tot}(f)}{10}}\right)$$

Therefore, the difference between the approximation and the exact model is:

$$T_{B,down_{simplified}}(f) - T_{B,down}(f) = \left(T_c - T_B(f, T_c)\right) 10^{-\frac{A_{tot}(f)}{10}}$$

As the frequency, f, increases, $T_B(f, T_c)$ tends towards 0 (note that $T_B(200\ GHz, T_c) = 0.2939$). As the frequency, f, decreases, $T_B(f, T_c)$ tends towards T_c. It implies that whatever the attenuation, *A*, on the slant path:

$$0 \leq T_{B,down_{simplified}}(f) - T_{B,down}(f) \leq T_c - T_B(f, T_c) \leq T_c$$

So, the approximation overestimates the exact brightness temperature with a maximum absolute error of 2.73 K, whatever the frequency and the total attenuation on the path. An illustration of such results is highlighted in Figure 4-3 where it is easy to get the maximum absolute error, $T_c - T_B(f, T_c)$, represented by the straight black line.

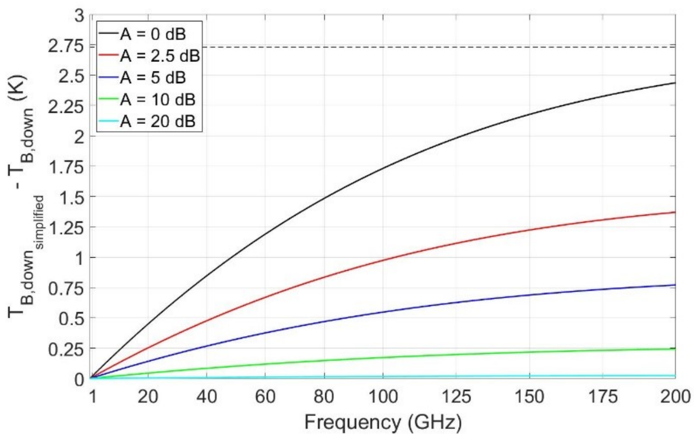

Figure 4-3 : Difference between the approximation and the exact model of brightness temperature

4.2 NEW PREDICTION METHOD OF THE INSTANTANEOUS DOWNWELLING BRIGHTNESS TEMPERATURE

4.2.1 METHODOLOGY TO DERIVE REFERENCE MAPS

Section 1 of Annex 1 of ITU-R P.676-12 [RD 2] is used to compute the oxygen specific attenuation profiles, $\gamma_o(Z)$, and the water vapour specific attenuation profiles, $\gamma_w(Z)$, from the worldwide total pressure, $P(Z)$, temperature, $T(Z)$, and water vapour density, $\rho_w(Z)$, profiles given by the new maps of the mean annual vertical atmospheric profiles provided in [RD 6] and briefly introduced in Section 2 of this document.

Section 1 of ITU-R P.840-8 [RD 5] is used to get the cloud liquid water specific attenuation profiles, $\gamma_c(Z) = K_l\big(T(Z)\big) \cdot \rho_l(Z)$ from the worldwide temperature, $T(Z)$, and cloud liquid water density, $\rho_l(Z)$, profiles given by the new maps of the mean annual vertical atmospheric profiles provided in [RD 6] and briefly introduced in Section 2 of this document. The cloud liquid water specific attenuation coefficient, K_l, is computed with the methodology described in Section 2 of ITU-R P.840-8.

Reference maps are then derived:

- Reference zenith total attenuation maps (oxygen + water vapour + clouds), $A_{tot_{ref}}$, from the integration of $\gamma(Z) = \gamma_o(Z) + \gamma_w(Z) + \gamma_c(Z)$ along the profiles according to the methodology described in Section 2 of Annex 1 of ITU-R P.676-12 [RD 2]
- Reference zenith downwelling microwave brightness temperature maps, $T_{B,down_{ref}}$, using the methodology described in Section 4.1.2 of this document
- Reference zenith mean radiating temperature maps, $T_{mr_{ref}}$, using the methodology described in Section 4.1.3 of this document

This process has been performed **from 1 to 200 GHz** (validity range of ITU-R P.840-8) with a frequency step of 1 GHz.

The reference zenith total attenuation maps at 20, 40, 50, and 80 GHz (frequencies currently used in SatCom systems) are shown in Figure 4-4.

The reference zenith downwelling microwave brightness temperature maps at 20, 40, 50, and 80 GHz are shown in Figure 4-5.

The reference zenith mean radiating temperature maps at 20, 40, 50, and 80 GHz are shown in Figure 4-6.

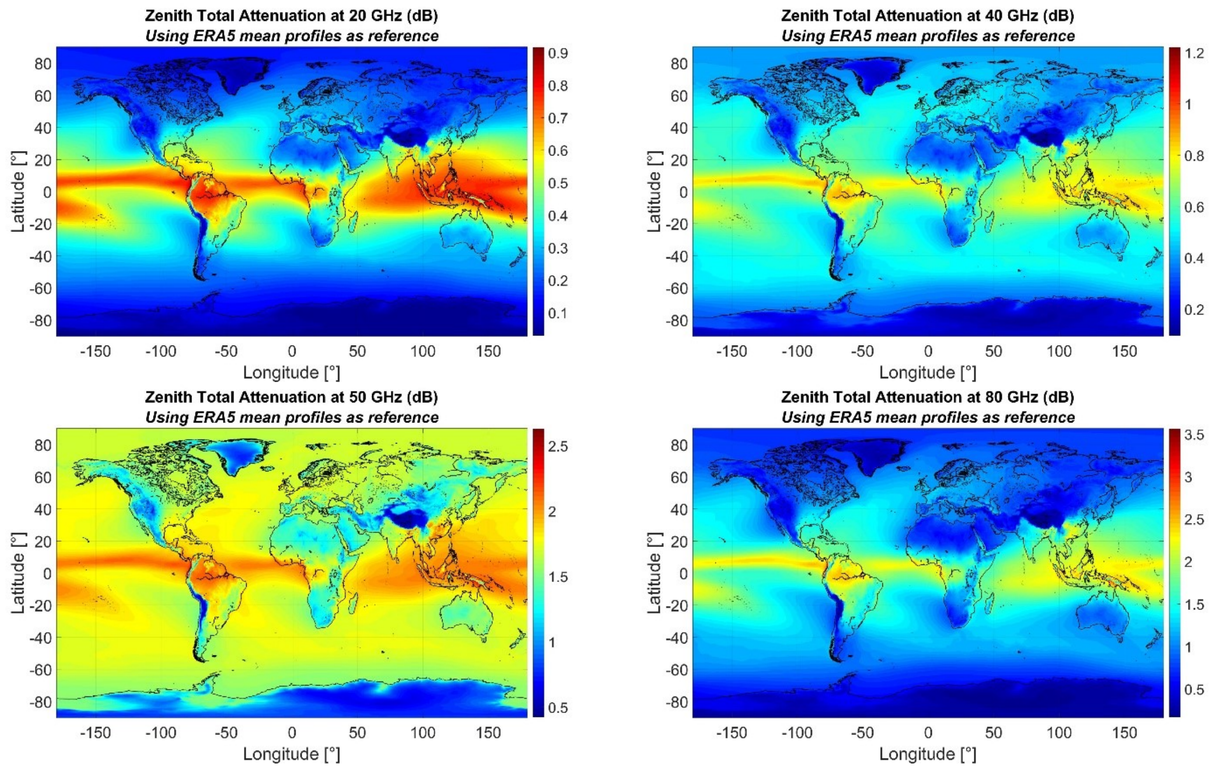

Figure 4-4 : Zenith total attenuation at 20, 40, 50, and 80 GHz derived from the integration of the oxygen, water vapour and cloud liquid water specific attenuation along the new ERA5 annual profiles by using Annex 1 of ITU-R P.676-12

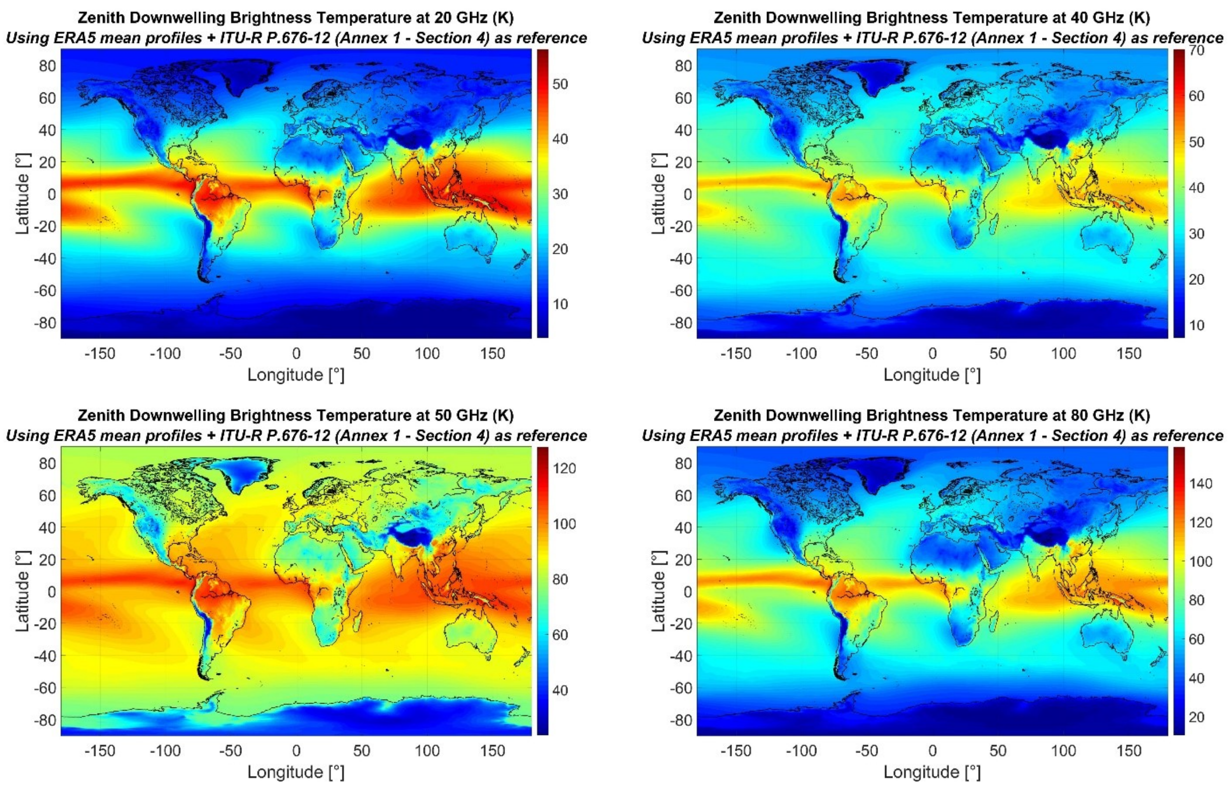

Figure 4-5 : Zenith downwelling microwave brightness temperature at 20, 40, 50, and 80 GHz derived with the new ERA5 annual profiles

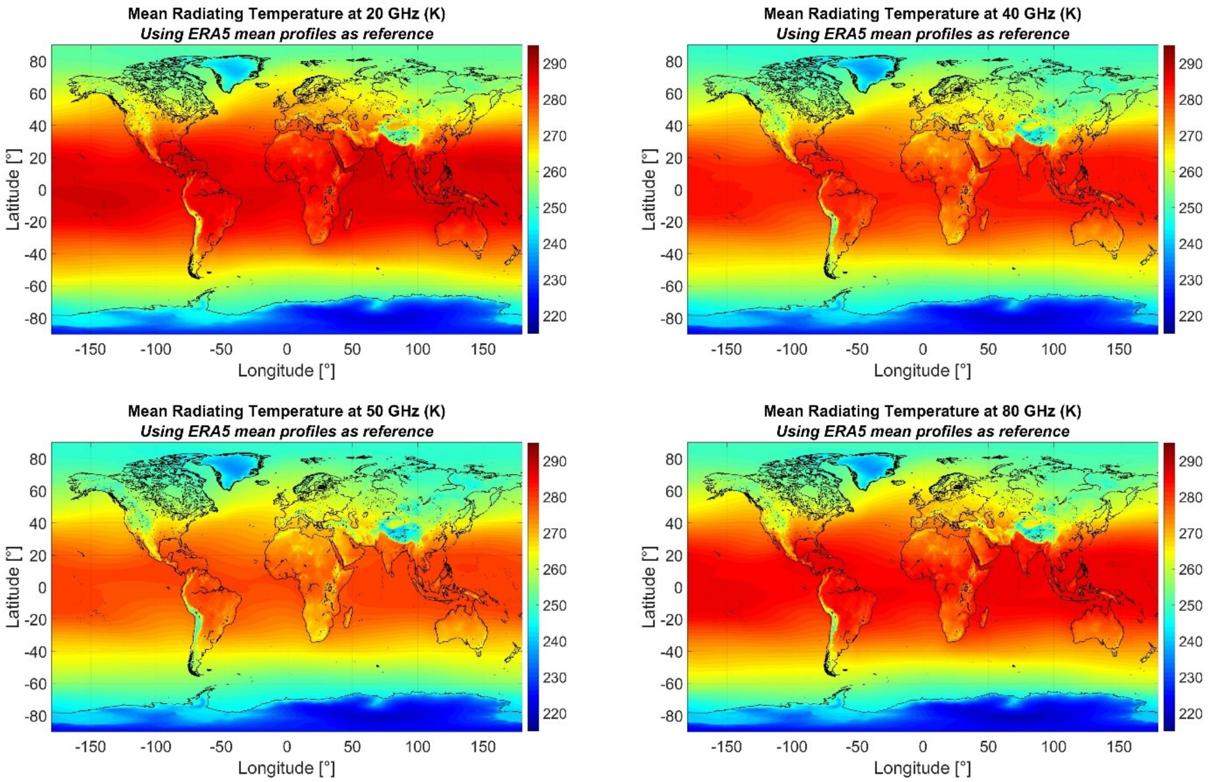

Figure 4-6 : Zenith mean radiating temperature at 20, 40, 50, and 80 GHz derived with the new ERA5 annual profiles

4.2.2 NEW MODEL OF THE MEAN RADIATING TEMPERATURE

4.2.2.1 DESCRIPTION

The idea is to propose a new model to compute the mean radiating temperature, T_{mr} (in K), such that net downwelling brightness temperature can be easily derived from:

$$T_{B,down}(f) = T_B(f, T_c)10^{-\frac{A_{tot}(f)}{10}} + T_{mr}(f)\left(1 - 10^{-\frac{A_{tot}(f)}{10}}\right)$$

where $T_B(f, T_c)$ is the planck adjustment on the exoatmospheric cosmic microwave background blackbody temperature, T_c. $A_{tot}(f)$ is the total attenuation, in dB, along the path in absorbing conditions.

The new proposed model has been derived by applying the following step-by-step procedure:

1. for each frequency, *f*, between 1 and 200 GHz, a global map of optimal values of $T_{mr_{ref}}(f)$, is computed as explained in Section 4.2.1
2. for each frequency, *f*, between 1 and 200 GHz, the best linear relationship between $T_{mr_{ref}}(f)$ and the surface total pressure, P_s (hPa), surface temperature, T_s (K), and surface water vapour density, ρ_{w_s} (g/m^3), is found. Four different models are tested:
   a. $T_{mr_{ref}}(f) = T_{mr_{ref}}(f, T_s) = a_t(f) + b_t(f) \cdot T_s$
   b. $T_{mr_{ref}}(f) = T_{mr_{ref}}(f, T_s, P_s) = a_t(f) + b_t(f) \cdot T_s + c_t(f) \cdot P_s$
   c. $T_{mr_{ref}}(f) = T_{mr_{ref}}(f, T_s, \rho_{w_s}) = a_t(f) + b_t(f) \cdot T_s + d_t(f) \cdot \rho_{w_s}$
   d. $T_{mr_{ref}}(f) = T_{mr_{ref}}(f, T_s, P_s, \rho_{w_s}) = a_t(f) + b_t(f) \cdot T_s + c_t(f) \cdot P_s + d_t(f) \cdot \rho_{w_s}$

   It has to be noticed that the linear regression has been performed by weighting each grid point (pixel) by the area on the surface of the Earth as explained in Section 3 of this document. Examples of the retrieval of the mean radiating temperature (using model d.) are given below:

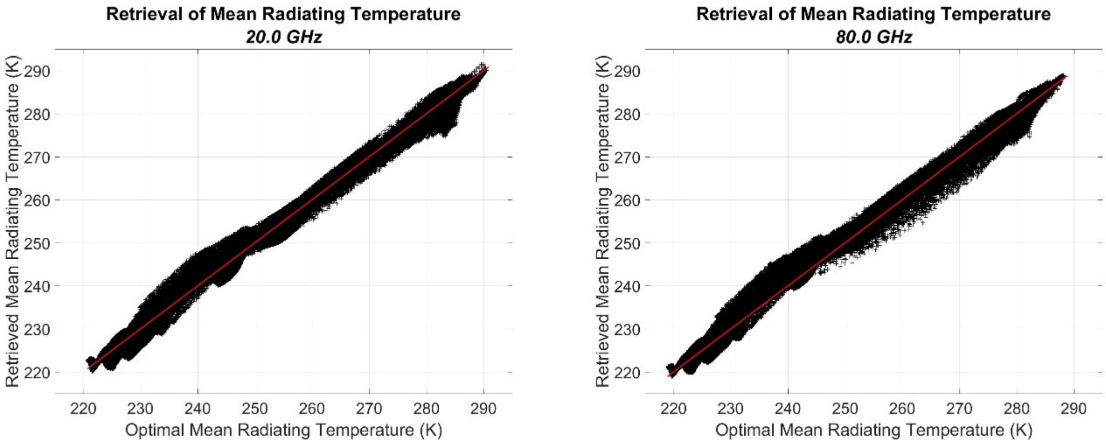

3. The absolute (in K) and relative (in %) RMS errors between the optimal mean radiating temperature and the proposed models are computed

The results of the linear regressions are given in Figure 4-7 where the specific values of the coefficients a_t, b_t, c_t, and d_t are highlighted.

The absolute and relative RMS errors between the optimal mean radiating temperature and the proposed models are shown in Figure 4-8. It can be observed that adding more surface parameters improves the global performances of the model.

Finally, for a given frequency, *f*, the final new prediction method of the instantaneous net downwelling brightness temperature is:

$$T_{B,down}(f) = T_B(f, T_c)10^{-\frac{A_{tot}(f)}{10}} + T_{mr}(f, T_s, P_s, \rho_{w_s})\left(1 - 10^{-\frac{A_{tot}(f)}{10}}\right)$$

with $T_{mr}(f, T_s, P_s, \rho_{w_s}) = a_t(f) + b_t(f) \cdot T_s + c_t(f) \cdot P_s + d_t(f) \cdot \rho_{w_s}$.

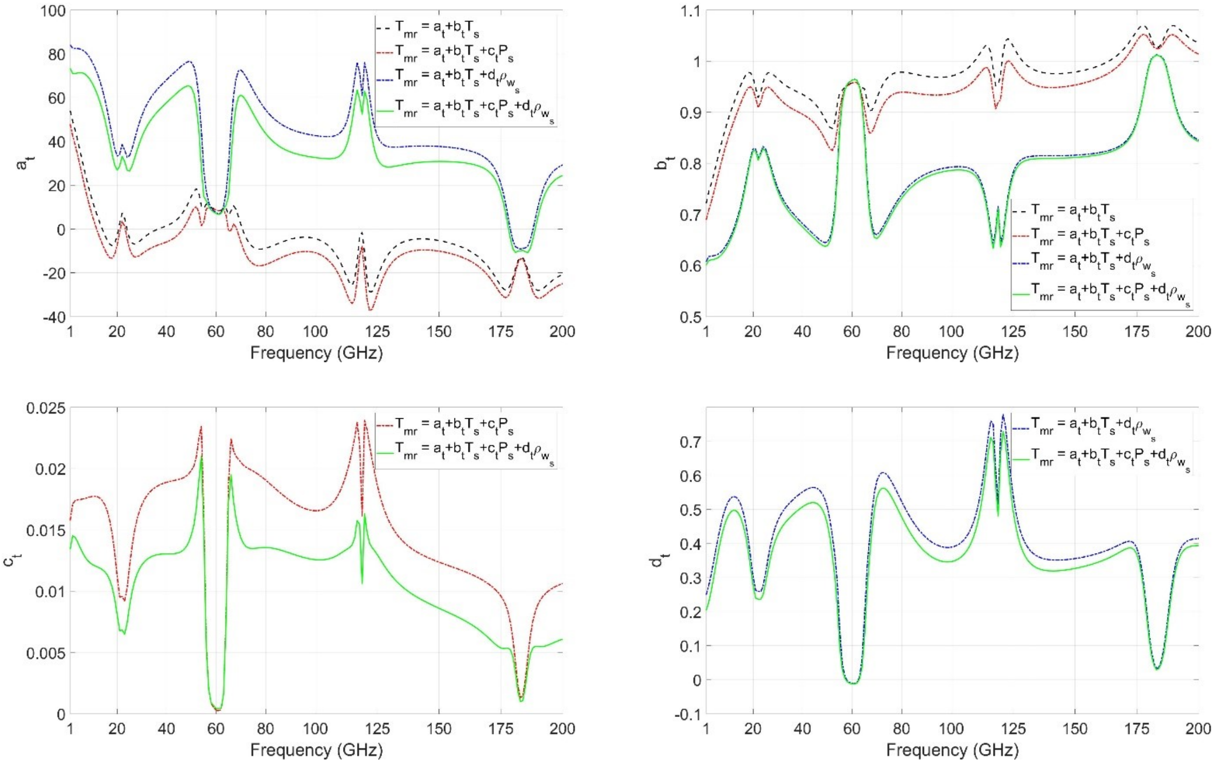

Figure 4-7 : a_t, b_t, c_t, and d_t coefficients of the new model of the mean radiating temperature

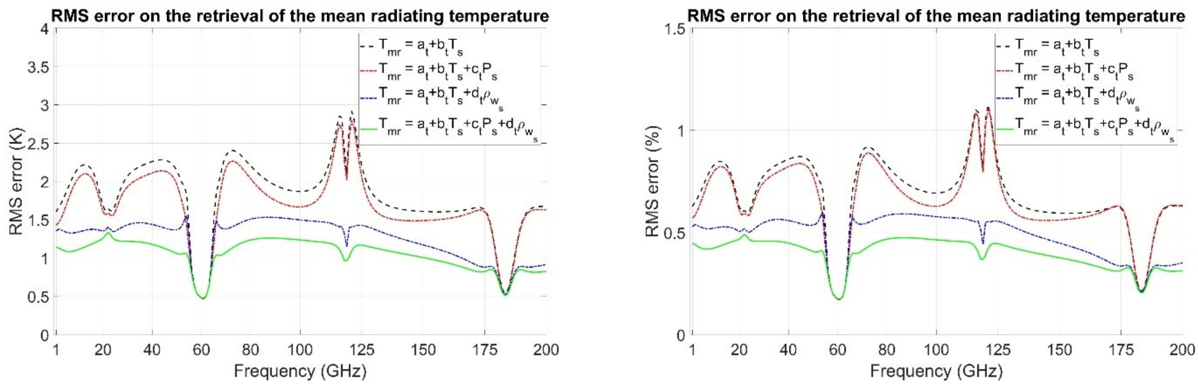

Figure 4-8 : Absolute (left) and relative (right) RMS errors of the new model of the mean radiating temperature

4.2.2.2 VERIFICATION AND COMPARISONS TO ITU-R P.676-11 AND ITU-R P.676-12

The prediction method of Section 3.2 of Part 3 of ITU-R P.372-14 and the new model have been tested using the new mean annual maps provided in [RD 6] and briefly introduced in Section 2 of this document.

First, the worldwide absolute and relative errors on the retrieval of the mean radiating temperature for the selected frequencies between 1 and 200 GHz are computed. Some illustrations of the relative errors at 20, 40, 50 and 80 GHz are shown in Figure 4-9. Figure 4-10 highlights the relative mean and RMS errors from 1 to 200 GHz. It can be observed that the new model performs largely better than Section 3.2 of Part 3 of ITU-R P.372-14 over the full range of frequency from 1 to 200 GHz. Indeed, the relative RMS errors for ITU-R P.372-14 are between 1% and 5%, while for the new model, it is always around 0.5%.

Then, the same work has been performed on the net downwelling brightness temperature. First, the worldwide absolute and relative errors on the retrieval of the net downwelling brightness temperature for the selected frequencies between 1 and 200 GHz are computed. Some illustrations of the relative errors at 20, 40, 50 and 80 GHz are shown in Figure 4-11. Figure 4-12 highlights the relative mean and RMS errors from 1 to 200 GHz. It can be observed that the new model performs largely better than Section 3.2 of Part 3 of ITU-R P.372-14 over the full range of frequency from 1 to 200 GHz. Indeed, the relative RMS errors for ITU-R P.372-14 are still between 1% and 5%, while for the new model, it is always around 0.5%.

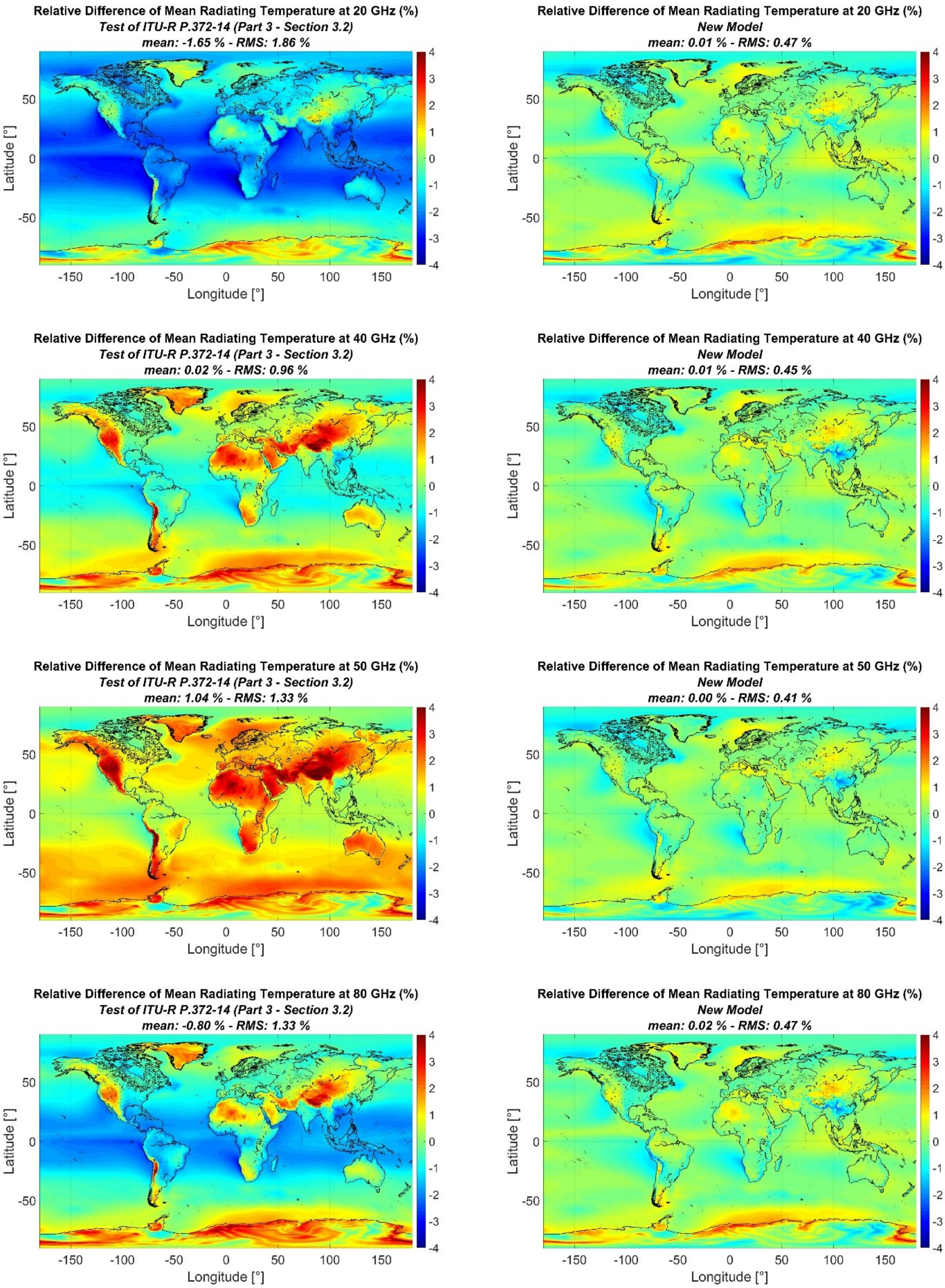

Figure 4-9 : Relative error of mean radiating temperature
1st line: 20 GHz, 2nd line: 40 GHz, 3rd line: 50 GHz, 4th line: 80 GHz
1st column: ITU-R P.372-14, 2nd column: new model

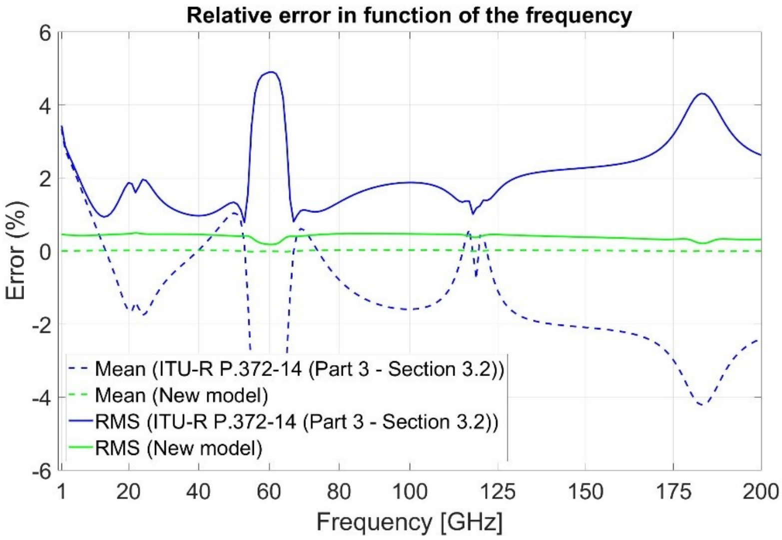

Figure 4-10 : Relative mean and RMS errors on the retrieval of the mean radiating temperature in function of the frequency

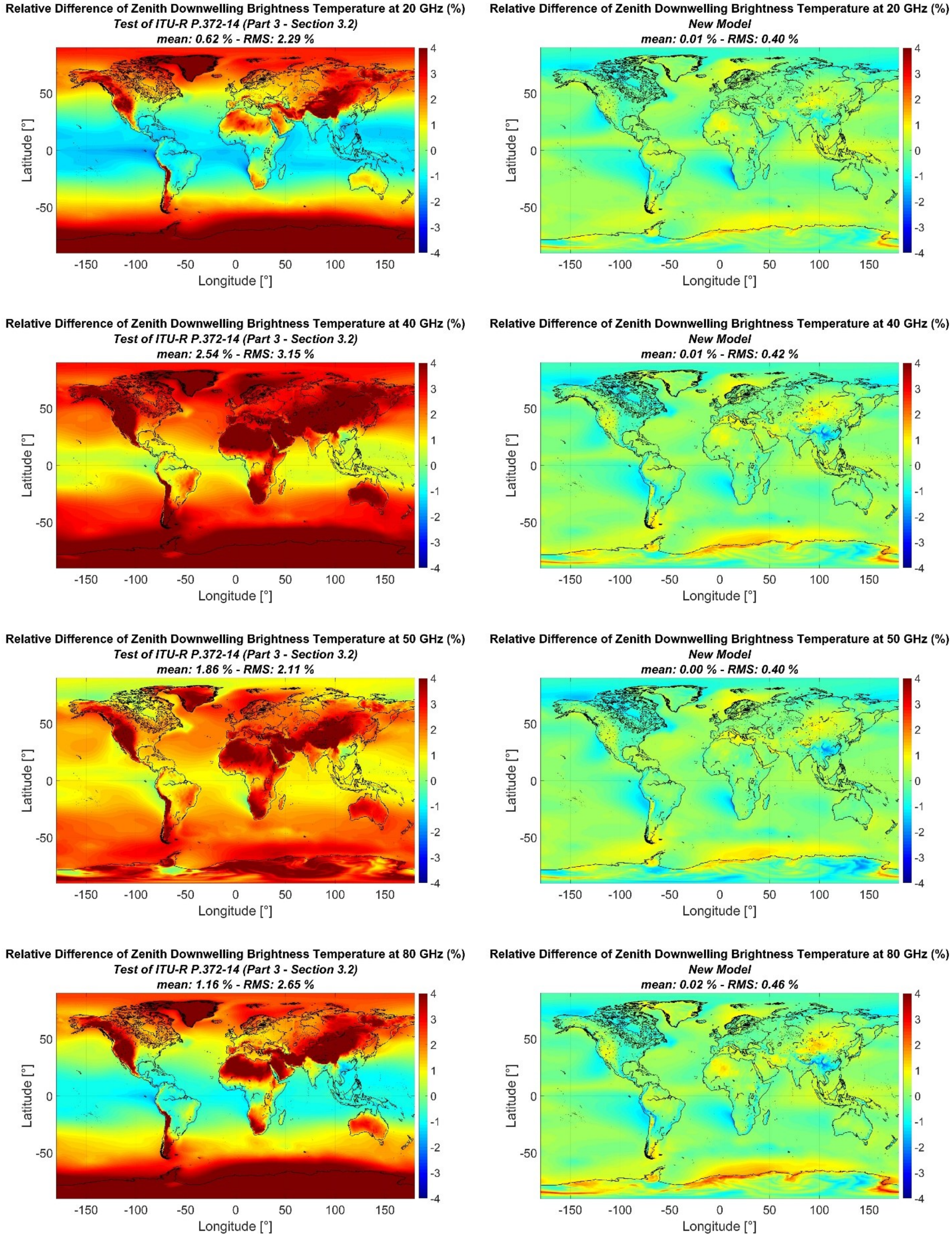

Figure 4-11 : Relative error of zenith downwelling brightness temperature
1st line: 20 GHz, 2nd line: 40 GHz, 3rd line: 50 GHz, 4th line: 80 GHz
1st column: ITU-R P.372-14, 2nd column: new model

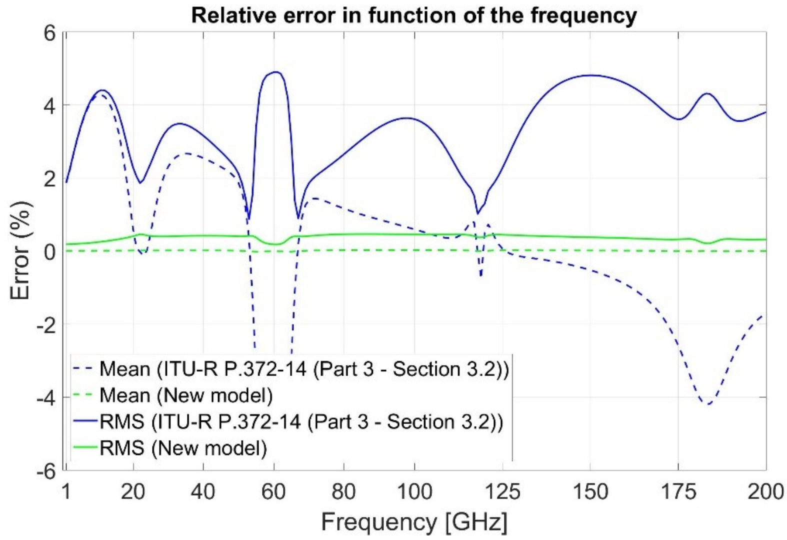

Figure 4-12 : Relative mean and RMS errors on the retrieval of the zenith downwelling brightness in function of the frequency

4.2.2.3 TEST USING RADIOSOUNDING OBSERVATIONS (RAOBS)

To test the performances of the new instantaneous net downwelling brightness temperature prediction method with respect to Section 3.2 of Part 3 of ITU-R P372-14, concurrent surface total pressure, surface temperature, surface water vapour density, mean radiating temperature, and total attenuation have been extracted from radiosounding observations (RAOBS) data. Ten years (2011-2020) of RAOBS on 24 different locations have been taken into account. As these RAOBS data were also used to test oxygen, water vapour and cloud attenuation prediction methods in [RD 6], only RAOBS for which the highest altitude level is above 25 km have been considered. The table below highlights the main information on the RAOBS dataset. The total number of RAOBS used is 80698.

Country (NOAA ID)	Site	Latitude (°N)	Longitude (°E)	Altitude (m)	Total number of RAOBS	Number of RAOBS with the highest level above 25 km
AR	BUENOS-AIRES-EZEIZA	-34.82	-58.53	20	4930	3635
AT	GRAZ	47.00	15.43	347	3106	1254
BR	GALEAO-RIO	-22.82	-43.25	6	6650	1980
CI	ABIDJAN-PORT-BOUET	5.25	-3.93	8	5569	1713
CN	BEIJING-PEKING	39.93	116.28	55	6558	677
ES	MADRID-BARAJAS	40.47	-3.58	638	6449	5637
FR	BORDEAUX-MERIGNAC	44.83	-0.70	45	6413	3267
GA	LIBREVILLE-LEON-MBA	0.45	9.42	15	2206	1037
GF	CAYENNE-ROCHAMBEAU	4.83	-52.37	9	6851	2728
GP	POINTE-A-PITRE-RAIZET	16.27	-61.52	8	4667	2247
GR	ATHENS-HELLENKION	37.90	23.73	14	2479	853
IN	CALCUTTA-DUM-DUM	22.65	88.45	6	8056	3774
IN	DELHI-SAFDARJUNG	28.58	77.20	216	9499	1537
IT	MILANO-LINATE	45.43	9.28	103	7447	6946
MX	MEXICO-CITY	19.43	-99.07	2309	7353	5073
NO	NY-ALESUND-II	78.92	11.93	8	4615	4292
PT	LISBON-GAGO-COUTINHO	38.77	-9.13	105	3208	1808
RE	SAINT-DENIS	-20.88	55.52	20	3221	1408
SG	SINGAPORE-CHANGI	1.37	103.98	16	11635	3993
US	DENVER	39.77	-104.88	1611	7270	6772
US	FAIRBANKS	64.82	-147.87	135	7264	6888
US	LAS-VEGAS	36.05	-115.18	693	7209	6553
US	MCMURDO-USA-BASE	-77.85	166.67	34	5270	225
US	MIAMI-INTL-UNIV	25.75	-80.38	4	7455	6401

As the cloud liquid water density profiles are not directly available from RAOBS, cloud detection algorithms must then be used. In the following analysis, the one described in the fascicle 3J/FAS/6 has been chosen.

First, the combined (for all sites) relative mean and RMS errors on the retrieval of the mean radiating temperature have been computed from 1 to 200 GHz with a frequency step of 1 GHz. The results are highlighted in Figure 4-13. It can be observed the new model performs better than Section 3.2 of Part 3 of ITU-R P.676-12 over the full range of frequency from 1 to 200 GHz.

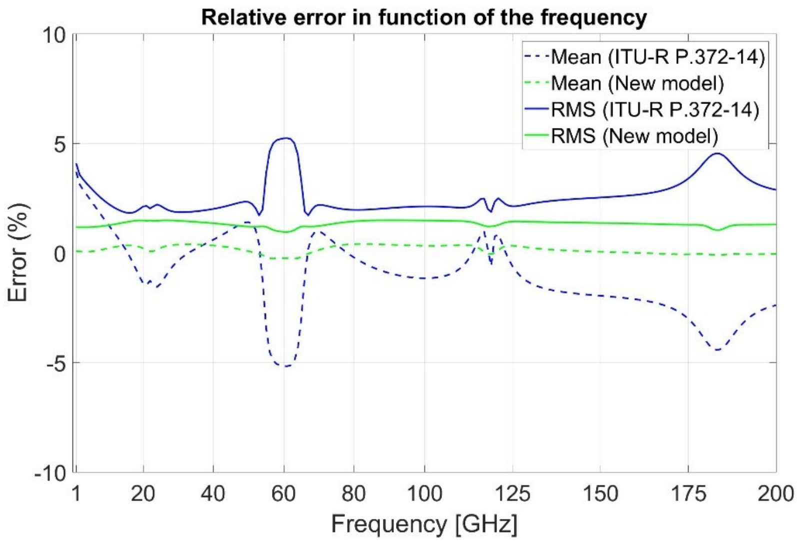

Figure 4-13 : Relative mean and RMS errors on the retrieval of the mean radiating temperature in function of the frequency

Second, the scatterplot of the retrieved mean radiating temperature vs. the reference mean radiating temperature is also a good performance indicator. The results at 20, 40, 80, and 150 GHz are shown in Figure 4-14. The straight black line represents the curve y=x. It can be then observed that the new model performs better than the in-force ITU-R prediction method which is in agreement with the results of Figure 4-13.

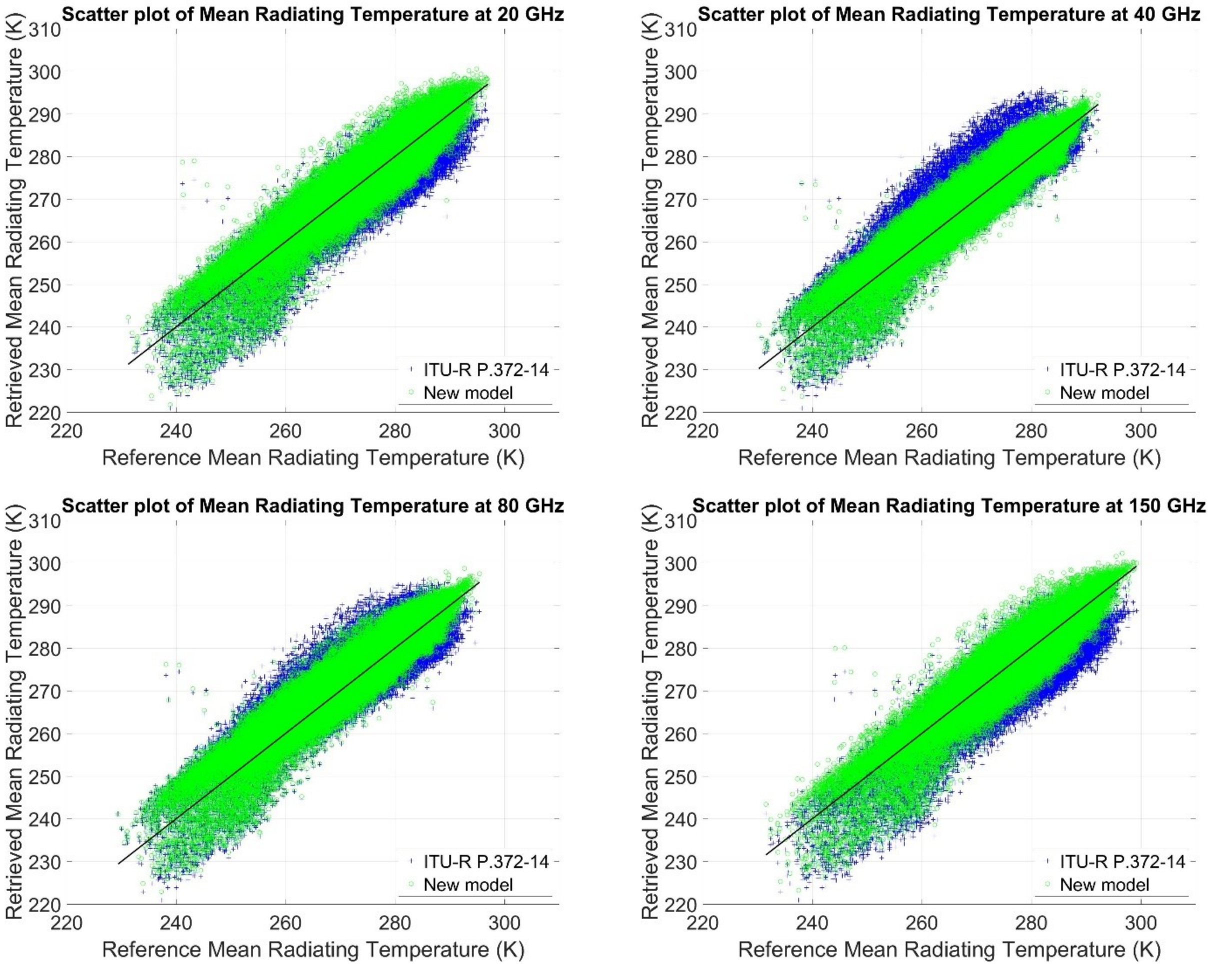

Figure 4-14 : Scatterplot of mean radiating temperature

Finally, CCDF of the mean radiating temperature (taking into account the full dataset, so disregarding the locations) have been computed. The results at 20, 40, 80, and 150 GHz are given in Figure 4-15. It can be observed a very good agreement of the new proposed model.

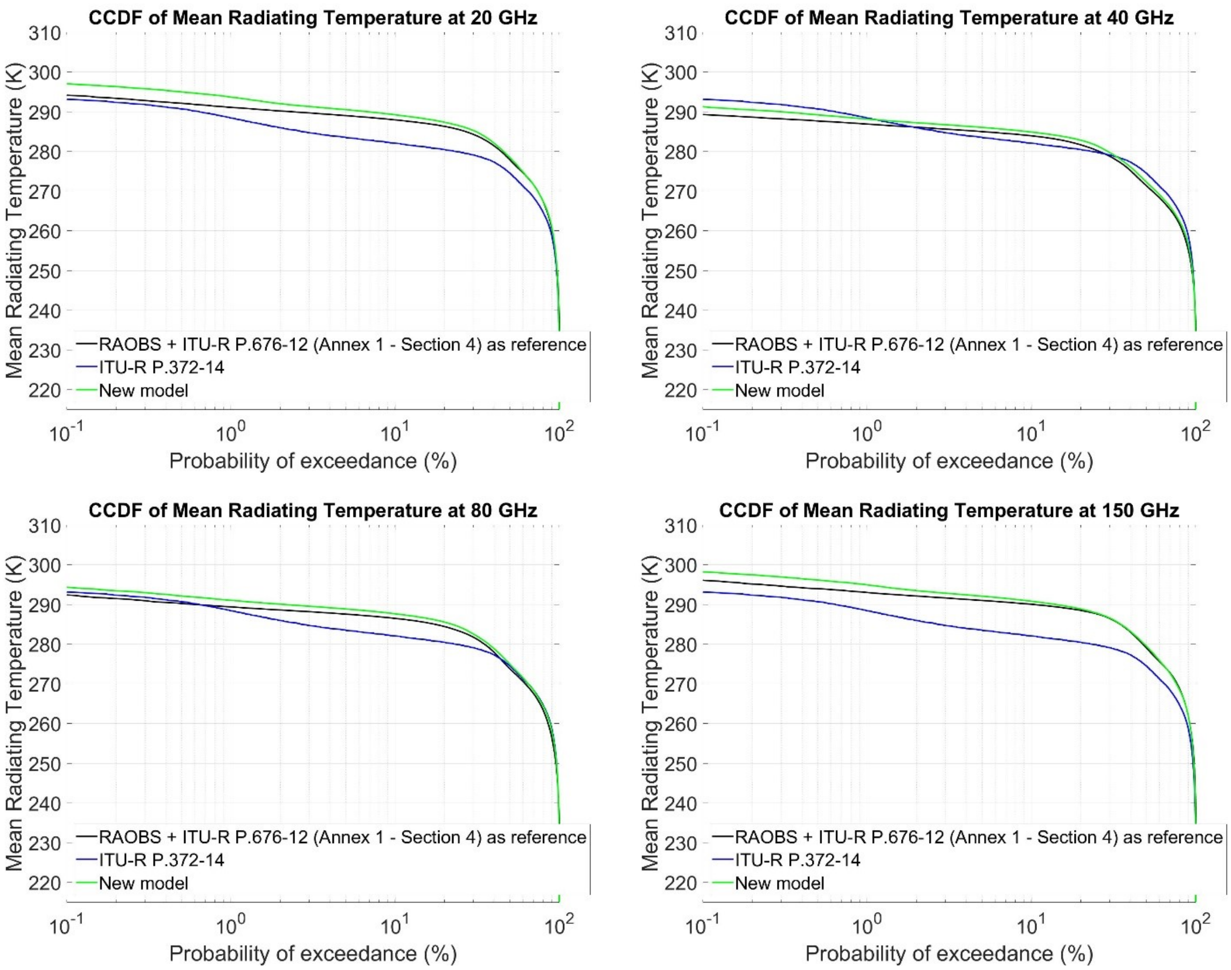

Figure 4-15 : CCDF of mean radiating temperature

The same work has been performed on the net downwelling brightness temperature. First, the combined (for all sites) relative mean and RMS errors on the retrieval of the net downwelling brightness temperature have been computed from 1 to 200 GHz with a frequency step of 1 GHz. The results are highlighted in Figure 4-16. It can be observed the new model performs better than Section 3.2 of Part 3 of ITU-R P.676-12 over the full range of frequency from 1 to 200 GHz.

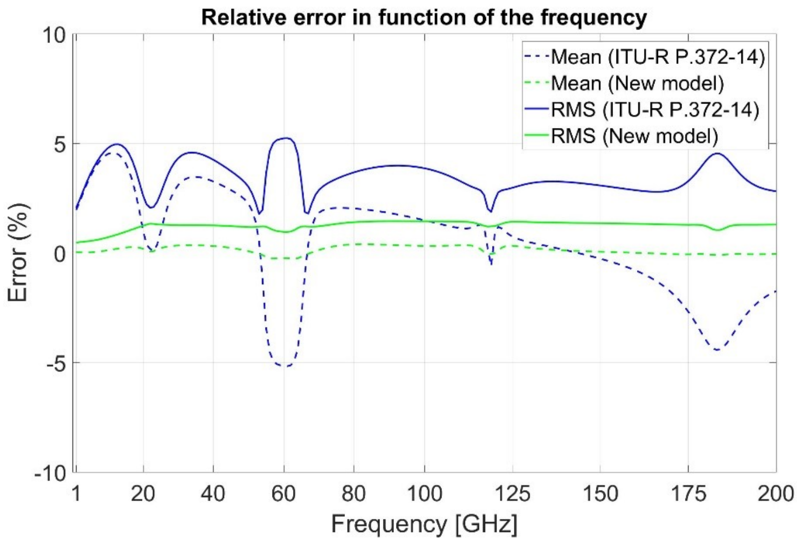

Figure 4-16 : Relative mean and RMS errors on the retrieval of the net downwelling brightness temperature in function of the frequency

Second, the scatterplot of the retrieved net downwelling brightness temperature vs. the reference net downwelling brightness temperature is also a good performance indicator. The results at 20, 40, 80, and 150 GHz are shown in Figure 4-17. The straight black line represents the curve y=x. It can be then observed that the new model performs better than the in-force ITU-R prediction method which is in agreement with the results of Figure 4-16.

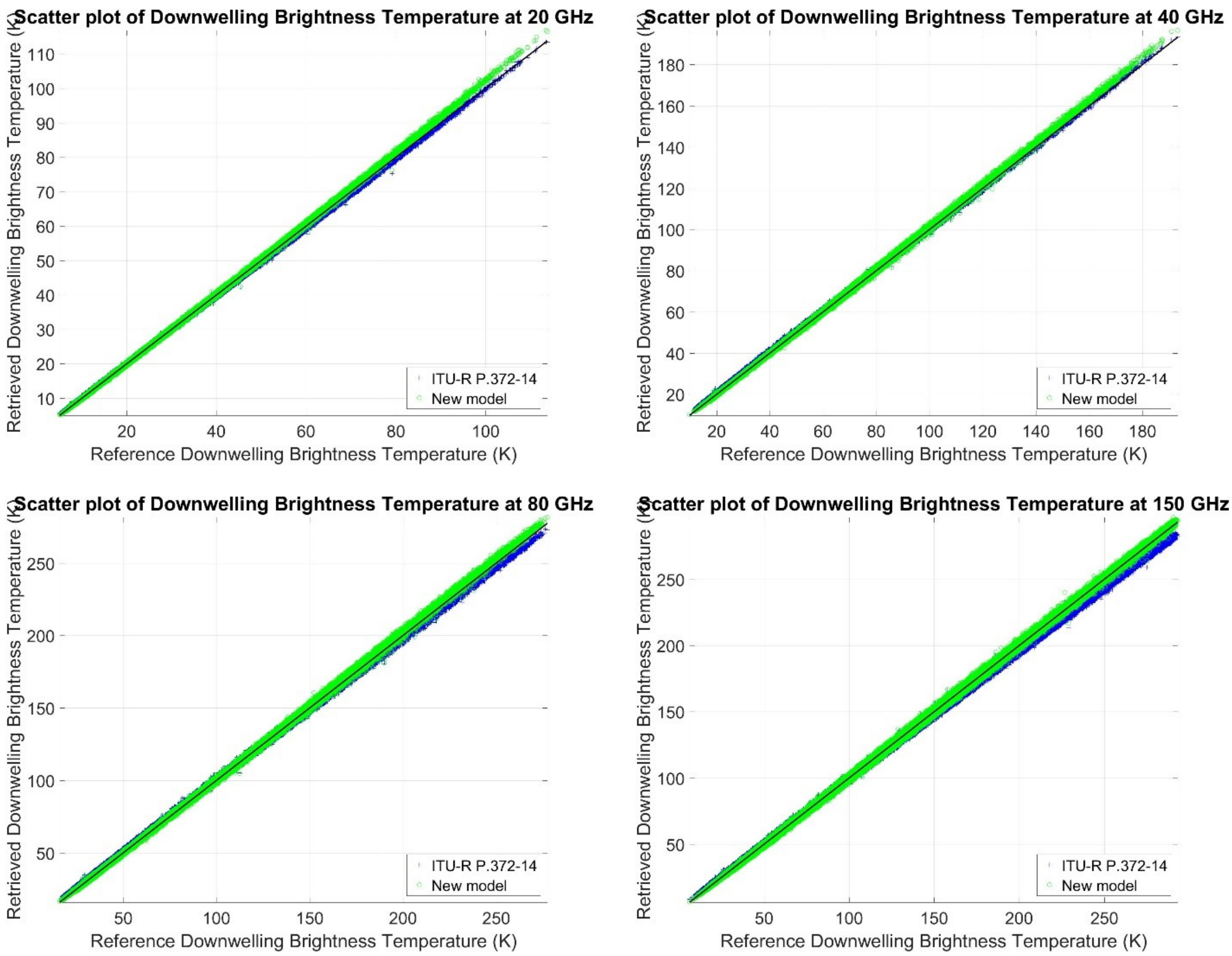

Figure 4-17 : Scatterplot of net downwelling brightness temperature

Finally, CCDF of the net downwelling brightness temperature (taking into account the full dataset, so disregarding the locations) have been computed. The results at 20, 40, 80, and 150 GHz are given in Figure 4-18. It can be observed a very good agreement of the new proposed model.

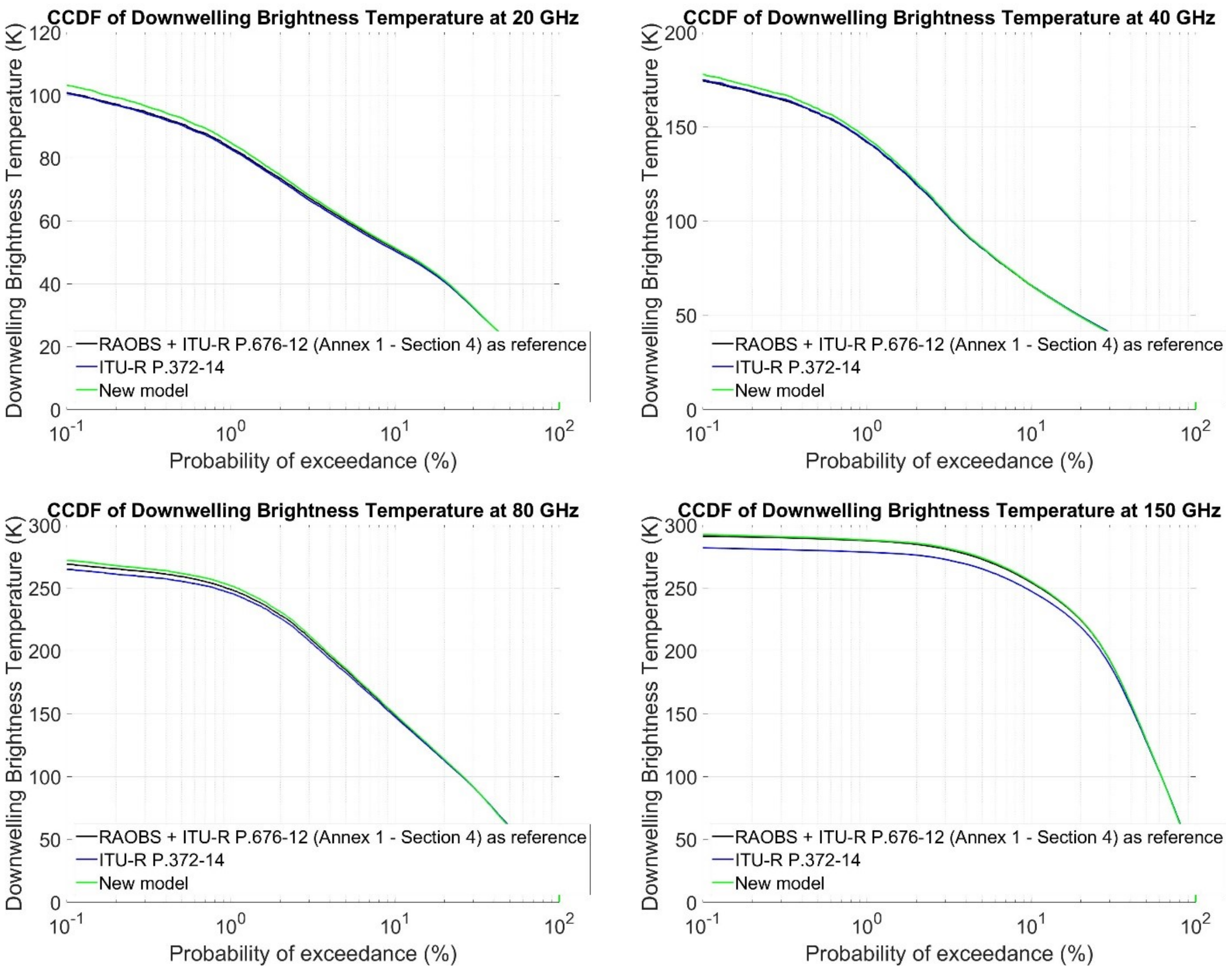

Figure 4-18 : CCDF of net downwelling brightness temperature

4.3 NEW PREDICTION METHOD OF THE STATISTICAL DISTRIBUTION OF DOWNWELLING BRIGHTNESS TEMPERATURE

Recalling that the new prediction method of the instantaneous net downwelling brightness temperature based on the mean radiating temperature is (section 4.2.2.1):

$$T_{B,down}(f) = T_B(f,T_c)10^{-\frac{A_{tot}(f)}{10}} + T_{mr}(f,T_s,P_s,\rho_{w_s})\left(1-10^{-\frac{A_{tot}(f)}{10}}\right)$$

with $T_{mr}(f,T_s,P_s,\rho_{w_s}) = a_t(f) + b_t(f)\cdot T_s + c_t(f)\cdot P_s + d_t(f)\cdot \rho_{w_s}$, it is not necessarily straightforward to define a new prediction method of the statistical distribution (CCDF) of net downwelling brightness, $T_{B,down}(f,p)$, temperature where *p* is the probability of exceedance (in %).

The proposed modelling of $T_{B,down}(f,p)$ is the following

$$T_{B,down}(f,p) = T_B(f,T_c)10^{-\frac{A_{tot}(f,p)}{10}} + T_{mr}(f,\overline{T_s},\overline{P_s},\overline{\rho_{w_s}})\left(1-10^{-\frac{A_{tot}(f,p)}{10}}\right)$$

with $T_{mr}(f,\overline{T_s},\overline{P_s},\overline{\rho_{w_s}}) = a_t(f) + b_t(f)\cdot \overline{T_s} + c_t(f)\cdot \overline{P_s} + d_t(f)\cdot \overline{\rho_{w_s}} = \overline{T_{mr}}(f)$.

$\overline{P_s}$, $\overline{T_s}$, and $\overline{\rho_{w_s}}$ are respectively the mean of surface pressure, surface temperature and surface water vapour density over the period of interest (e.g. annual or monthly mean). $A_{tot}(f,p)$ represents the CCDF of total attenuation (in absorbing conditions) over the same period of interest (e.g. annual or monthly CCDF), i.e. the values of A_{tot} exceeded for *p* % of the time.

Examples for some RAOBS sites are given in the following figures where the results coming from the instantaneous prediction method are compared with the results coming from the statistical prediction method. Figure 4-19 shows some comparisons of instantaneous and statistical prediction methods of the downwelling brightness temperature at 40 and 80 GHz. The black curve is the reference coming from the exact computation on RAOBS.

When local data of $\overline{P_s}$, $\overline{T_s}$, $\overline{\rho_{w_s}}$, and $A_{tot}(f,p)$ are not available, [RD 6] provides to the user digital tabulated worldwide maps of $\overline{P_s}$, $\overline{T_s}$, and $\overline{\rho_{w_s}}$, and prediction methods of $A_{tot}(f,p)$ to be able to predict the CCDF of the net downwelling brightness temperature anywhere in the world.

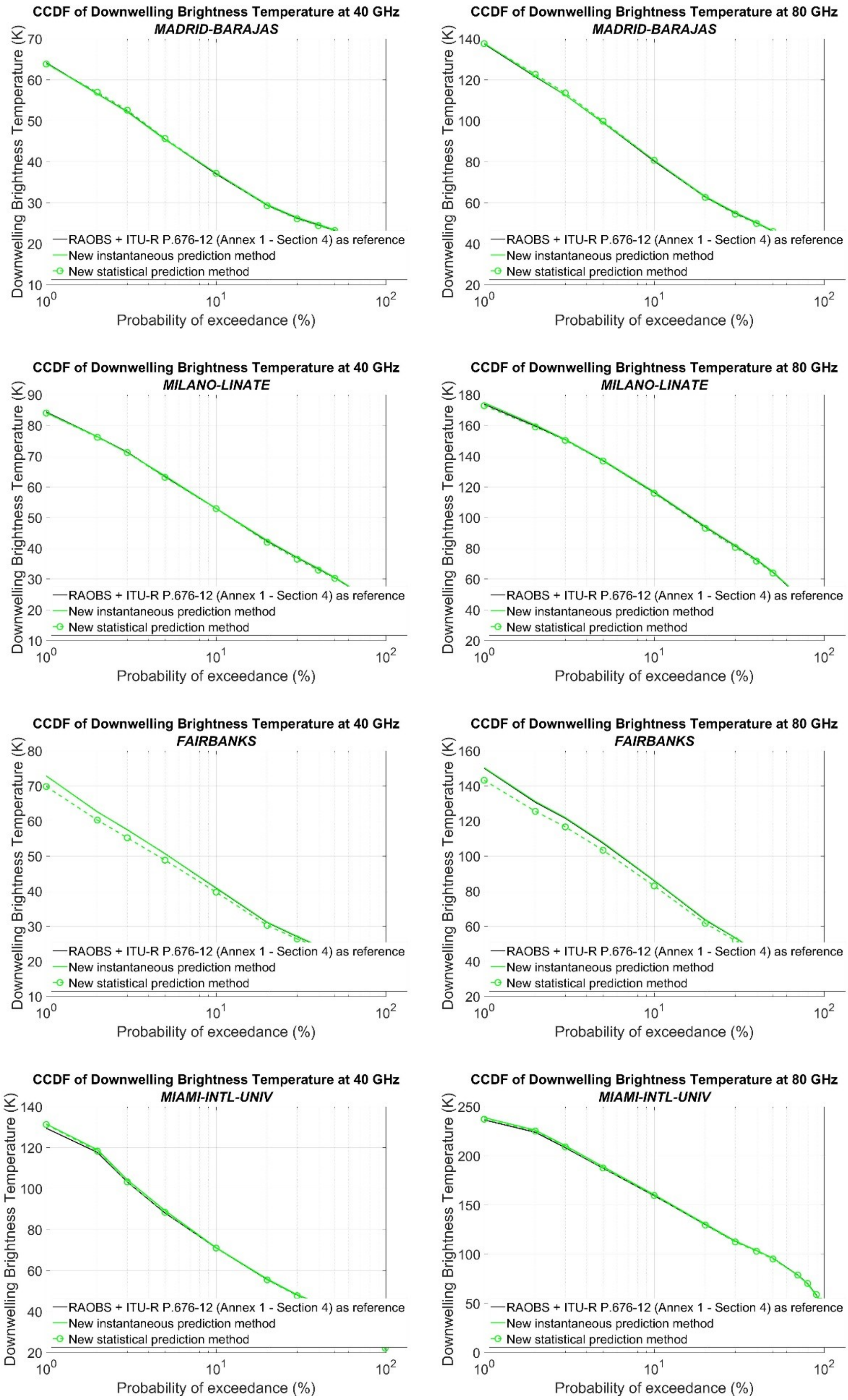

Figure 4-19 : Comparisons of instantaneous and statistical prediction methods of net downwelling brightness temperature
left: 40 GHz, right: 80 GHz

5 CONCLUSIONS

In this document, a synthesis of the CNES internal research activities on downwelling brightness temperature models for Earth-Space paths between 1 and 200 GHz has been given:

- a new model to compute the **mean radiating temperature** in clear sky and cloudy conditions has been proposed. It allows the **instantaneous net downwelling brightness temperature** to be retrieved. It shows better performances than the prediction method recommended in ITU-R P.372-14 while enlarging its validity domain
- then, a new model to compute the **statistical distribution of the net downwelling microwave brightness temperature from the statistical distribution of total attenuation on the slant path** has been derived. It shows a perfect agreement when compared with the performances of the new instantaneous prediction method.

6 REFERENCES

[1] https://cds.climate.copernicus.eu/cdsapp#!/dataset/reanalysis-era5-single-levels?tab=overview

[2] https://confluence.ecmwf.int/display/CKB/ERA5%3A+data+documentation

7 ACKNOWLEDGEMENT

The author would like to thank the colleagues from the ITU-R SG3 Correspondence Groups CG 3J-1, CG 3J-11 and CG 3J-3M-5 and in particular Harvey Berger, Antonio Martellucci, Carlo Riva, Lorenzo Luini, and George Brost for their support in the CNES propagation activities. The author is also very grateful to the colleagues from ONERA for checking the work.

END OF DOCUMENT